

# Age and Metallicity Effects in $\omega$ Centauri:

## Stromgren Photometry at the Main-Sequence Turn-Off

Joanne Hughes <sup>1 2</sup> and George Wallerstein

e-mail contact: [hughes@astro.washington.edu](mailto:hughes@astro.washington.edu)

Department of Astronomy, University of Washington, Box 351580, Seattle, WA 98195-1580

Received \_\_\_\_\_;    accepted \_\_\_\_\_

---

<sup>1</sup>Visiting astronomer, Cerro Tololo Inter-american Observatory, operated by the National Optical Astronomy Observatory under contract to the National Science Foundation.

<sup>2</sup>Now at: Physics Department, Everett Community College, 801 Wetmore Avenue, Everett, WA 98201

## ABSTRACT

We have observed (with *vby* filters) a field north of the core of the most massive globular cluster in our galaxy,  $\omega$  Centauri. We have found a correlation of age and metallicity in a region which avoids the dense core and the inhomogeneous foreground dust emission shown by the IRAS satellite. Our observations show that the comparatively metal-rich stars (as defined by the  $(b - y)$  and  $m_1$  colors) are younger than the metal-poor stars by at least 3 Gyr. This correlation of metallicity with age suggests that  $\omega$  Cen has enriched itself over a timescale of about 3 Gyr, and possibly longer. It is remarkable that ejecta from stellar winds combined with supernovae of type II failed to disperse the cluster's interstellar matter at an earlier epoch, but were captured by the cluster instead. Star formation would have ceased as type Ia supernovae dispersed the remaining interstellar matter. This work and other recent evidence suggests that  $\omega$  Cen could have been part of a small satellite galaxy in which all the activity occurred before it was captured by the Milky Way.

Key words: (Galaxy:) globular clusters: individual: ( $\omega$  Cen, NGC 6397) — techniques: photometric

## 1. Introduction

The most massive ( $3 \times 10^6 M_\odot$ ), and flattened ( $e = 0.8$ ) globular cluster in our galaxy,  $\omega$  Centauri (NGC 5139), is known to show a wide range of metallicity among both its RR Lyrae stars (Butler, Dickens and Epps 1978) and its red giants (Norris and Da Costa 1995). The full range of metallicity is approximately  $-2.0 < [Fe/H] < -0.5$ , with relatively few stars showing  $[Fe/H] > -1.0$ . The question of whether this unusual inhomogeneity in chemical composition is caused by self-enrichment, a chemically-diverse parent cloud, the capture of  $\omega$  Cen from a satellite system, or the formation of the cluster by a merger event, has been the topic of much discussion (see discussion in Vanture, Wallerstein and Brown 1994, Norris *et al.* 1997). Additionally, the absolute ages of globular clusters are important because they provide a lower limit to the age of the universe (Gratton *et al.* 1997). In the case of  $\omega$  Cen, evidence of the spread in age and/or metallicity gives clues to the chemical enrichment of our galaxy. The origin of the chemical composition diversity in  $\omega$  Cen is not only an intriguing problem itself: its solution may be helpful in developing an understanding of the evolution of galaxies, especially ellipticals and the bulges of spirals (which may also show a range in metallicity).

The distribution of stars as a function of metallicity in  $\omega$  Cen has been investigated by two groups (Norris *et al.* 1996, and Suntzeff and Kraft 1996). The former group found the peak in the metallicity distribution at  $[Ca/Fe]=-1.7$ , and a second minor peak at  $[Ca/Fe]=-0.9$ . The latter group found that a single distribution fit the data with a peak at  $[Fe/H]=-1.7$  (which corresponds to  $[Ca/Fe]=-1.4$ ), and an asymmetric tail to higher metallicities, but no secondary maximum. Recently, Norris *et al.* (1997) cited evidence from 400 red giants, correlating kinematics with metal abundance. However, their data analysis could not differentiate between the  $\omega$  Centauri metal-poor component being older or younger than the metal-rich component, but the metal-rich and metal-poor stars do

appear to have substantially different kinematics, suggesting a merger event. Norris *et al.* (1997) use the Carina dwarf spheroidal system as their example of a system with about  $10^7 M_\odot$  of stars with four components of the stellar population differing in ages by several billion years. Could  $\omega$  Centauri have been part of a larger (dwarf galaxy) system which merged with the Milky Way (Freeman 1993, Dinescu *et al.* 1999)?

Morgan and Lake (1989) model  $\omega$  Centauri as a clear case of self-enrichment, and the question immediately arises as to over what timescale the enrichment took place. The Morgan and Lake model has been extended by Brown *et al.* (1991) and Parmentier *et al.* (1999). Can we detect a correlation between abundance and age in  $\omega$  Centauri? Alcaino and Liller (1987) suggest that the abundance variations are primordial, since they persist for both evolved and unevolved stars. Mukherjee *et al.* (1992, using a  $3' \times 5'$  field,  $20'W$  of the center of the cluster) found evidence for a maximum age spread of  $2 \times 10^9$  years and concluded that the metallicity spread at the turn-off was consistent with little spread in age (but that their constraint was weak). Evans (1983) suggested that the metal-rich stars in  $\omega$  Cen were born with their excesses of s-process species, rather than having generated them internally.

Since it is difficult to recognize an age-abundance correlation among the giants or RR Lyrae stars alone, we have analyzed the main-sequence turn-off (MSTO), where theoretical isochrones separate according to age (at a given metallicity). At least two colors (or color differences) must be measured for the stars, one that reveals the age and one that correlates with  $[Fe/H]$ ; the best system designed for this is Strömgren photometry. The Strömgren intermediate-band system (Strömgren 1966) has four primary filters (*uvby*) whose passbands were designed to measure the temperature, metallicity and gravity of a star (earlier than spectral-type G). In this paper, we utilize the metallicity index  $m_1 = (v - b) - (b - y)$ . The *y*-filter is usually converted to the Johnson V, and the  $(b - y)$ -index is related to

temperature. The *uvby* filters usually necessitate large numbers of long exposures on large telescopes (see method detailed in Folgheraiter *et al.* 1995), mostly because the stars of interest are faint at the *u*-band. However, our method circumvents the need for long *u*-exposures<sup>3</sup> with a 0.9-m telescope. We can reach almost the same faint-limit as the Mukherjee *et al.* (1992) study with the CTIO 4.0-m by avoiding the *u*-band. The  $m_1$ -indices of stars near the MSTO of a globular cluster are sensitive to metallicity. In the range  $-2.0 < [Fe/H] < -0.5$ , the slope of the  $m_1$  versus  $[Fe/H]$  is  $\Delta[Fe/H] = 0.056m_1$  (Schuster and Nissen 1989). Hence, we expect a total range in  $m_1$  of 0.084 magnitudes.

The models of VandenBerg and Bell (1985) and Vandenberg *et al.* (1999) show that, at the MSTO (which is at  $V \sim 18.3$  mag. for  $\omega$  Centauri), the color-magnitude diagram is nearly vertical. At the MSTO the color index ( $b - y$ ) is sensitive to age with a slope given by  $\Delta(b - y) = 0.010\Delta age(Gyrs)$  between 10 and 15 Gyrs. Hence, we can determine the metallicity of the stars using the  $m_1$ -index, divide them into groups of relatively low, medium and high metallicity, and compare them with the appropriate isochrones. The new Vandenberg *et al.* (1999) isochrones, with increased  $[\alpha/Fe]$  ratio, corrects differences in color which were seen with the previous models because an enhanced  $\alpha$ -element abundance makes colors redder and magnitudes fainter (Reid 1997).

We have been careful in selecting our field ( $\sim 25'$ N of the cluster center) to avoid the foreground dust emission shown in IRAS skyflux images (Wood and Bates 1993, 1994), which could be responsible for variable extinction across the face of the cluster. A y-image (1500s integration) of our  $\omega$  Cen field is shown in Figure 1.

We took exposures in a field away from the cluster (about  $1^\circ$  west of our cluster

---

<sup>3</sup>Folgheraiter *et al.* (1995) note that the *u*-band is at a wavelength where little light is emitted by red stars in globular clusters and that CCDs are not very sensitive here.

field, at approximately the same galactic latitude) to subtract field stars statistically. The color-magnitude diagram of stars in the off-cluster field does not show evidence of the cluster population (Figure 3b). In an effort to determine the effects of observational uncertainties, we utilized observations of NGC 6397 (taken during the same 0.9-m run), which were deliberately of poorer quality than that for  $\omega$  Cen. Hence, we performed tests to see if a single-metallicity cluster might show an age spread independent of the metallicity spread (Anthony-Twarog, Twarog and Suntzeff 1992) and mimic  $\omega$  Cen.

## 2. Observations

The observations were carried out with the CTIO 0.9-m telescope in May 1996. We used the Tek 2048 #3 chip (and Arcon 3.3) which gives a pixel size of  $0''.396$  (focal ratio:  $f/13.5$ ; pixel size:  $24\mu m$ ). The read noise was  $3.6e^-$  and the gain in  $e^-/ADU$  was 1.6. The instrument-control gain was on the #4 setting (which gave full-well at approximately 65,000 ADU), because our main project involved observations of globular cluster stars above and below the MSTO and a large dynamic range of magnitudes was needed. The theoretical field size is  $13'.5 \times 13'.5$ , but the Strömgren filters used at the time were  $2 \times 2$  inches (instead of  $3 \times 3$  inches for the broadband filters) and caused vignetting, so the effective field of view was reduced to about  $12'.0 \times 12'.0$ . The frames used for the analysis are listed in Table 1. This region includes the field used for the Eggen photo-electric sequence (Plate I, *Astronomer Royal*, ROA #2, 1966).

We used Strömgren standards from the E-regions (Kilkenny and Laing 1992), supplemented by some metal-deficient giants from Anthony-Twarog and Twarog (1994). The images were flatfielded using twilight sky-flats, accompanied by a sequence of 25 zeros. The images were then processed using the IRAF routine QUADPROC (to take into account the 4 amplifiers used on this system).

The FWHM of stars in all the images was  $1''.4$ – $2''.3$ . We used the DAOPHOT program in IRAF (Stetson, Davis and Crabtree 1990) to perform the crowded field photometry including two iterations of (DAOFIND-PHOT-ALLSTAR) with a  $4\sigma$ -detection threshold on the first pass through the program, then a  $5\sigma$ -detection limit on the second pass. The thresholds were set to get the best possible photometry at the MSTO, not to detect every possible stellar image on the frames. Point spread functions (PSFs) were constructed using 20-50 uncrowded stars in each image and the PSF was allowed to vary quadratically across the chip (although the degree of non-uniformity was small). The objects detected by ALLSTAR were then further selected by requiring that they have a  $\chi^2$  value between 0.5 and 1.5 (so that only *real* stars are picked, avoiding cosmic rays or extended objects).

Conversion from the instrumental magnitudes was achieved using the standards mentioned above with the following equations for 05/10/96.

$$(b - y) = 0.956(b - y)_i + 0.069(b - y)_i X - 0.066X - 0.069, \sigma_{rms} = 0.003 \quad (1)$$

$$V = y_i - 4.065 - 0.059X - 0.164(b - y)_i X + 0.236(b - y)_i, \sigma_{rms} = 0.005 \quad (2)$$

$$(v - b) = 0.872(v - b)_i - 0.014(v - b)_i X - 0.030X - 0.323 + 0.167(b - y)_i, \sigma_{rms} = 0.005 \quad (3)$$

Where  $X$  is airmass and the subscript  $i$  denotes the instrumental magnitudes.

On 05/09/96, 05/12/96 and 05/14/96, we found that for the Strömgren filters, using the additional  $constant \times (b - y)_i X$  term produced a greater scatter, so the transformations for the Strömgren observations on these nights were:

05/09/96:

$$(b - y) = 1.080(b - y)_i - 0.054X - 0.121, \sigma_{rms} = 0.007 \quad (4)$$

$$V = y_i - 3.996 - 0.123 + 0.013(b - y)_i, \sigma_{rms} = 0.007 \quad (5)$$

$$(v - b) = 0.980(v - b)_i - 0.104X - 0.278, \sigma_{rms} = 0.010 \quad (6)$$

05/12/96:

$$(b - y) = 1.036(b - y)_i - 0.011X - 0.136, \sigma_{rms} = 0.011 \quad (7)$$

$$V = y_i - 3.996 - 0.146X + 0.106(b - y)_i, \sigma_{rms} = 0.004 \quad (8)$$

$$(v - b) = 0.975(v - b)_i - 0.002X - 0.395, \sigma_{rms} = 0.010 \quad (9)$$

05/14/96:

$$(b - y) = 1.054(b - y)_i - 0.011X - 0.100, \sigma_{rms} = 0.007 \quad (10)$$

$$V = y_i - 3.979 - 0.121X + 0.043(b - y)_i, \sigma_{rms} = 0.011 \quad (11)$$

$$(v - b) = 0.980(v - b)_i - 0.096X - 0.255, \sigma_{rms} = 0.019 \quad (12)$$

The rms scatter for the transformation equations indicates that the nights were photometric with the least scatter being on 05/10/96. We determined the aperture correction between the small (5 pixel) aperture used by ALLSTAR and the larger aperture used on the standards by cleaning and examining the stars used to make the PSF in each image. Before eliminating any stars from the data set because of bright neighbors or larger errors, we note that after transforming  $y$  to  $V$ , the average uncertainty at  $18^{th}$  magnitude is better than 1%, and it is better than 3% at  $21^{st}$  magnitude.

We used the IMMATCH routines in IRAF to compare lists of objects detected in each frame, resulting in several data sets in  $vby$ , which we have then analyzed to form a coherent picture of this region. The  $\omega$  Cen working data set was chosen in the following way. Taking all the  $\omega$  Cen frames in Table 1, Figure 2 shows the uncertainties in  $m_1$  (Figure 2a and 2d),  $(b - y)$  (Figure 2b and 2e) and  $V$  (Figure 2c and 2f). The left-hand panels show



10981 sources which had detections in *any* vby images from Table 1. The uncertainties are calculated in quadrature from the photon statistics and how well DAOPHOT did the processing, the aperture corrections and the standard photometric errors. The right-hand panels in Figure 2 show the 2147 objects which were detected in all the frames (except the 300s exposures on 5/9/96), with the magnitudes and colors calculated as the weighted-means of each individual detection. We can see that the errors are significantly smaller for this restricted sample. For the NGC 6397 data, we selected sources (detected in the frames in Table 1) which had uncertainties,  $\sigma_{m_1} \leq 0.05$ ,  $\sigma_{b-y} \leq 0.02$  and  $\sigma_V \leq 0.015$ . Deliberately, we did not use weighted means here so that we would broaden the width of the upper main-sequence and MSTO regions.

### 3. Cluster Cleaning

In the absence of kinematic data, we have to rely on a statistical method to remove non-members from the clusters. To the data selected in Figure 2 for  $\omega$  Cen, we added the shorter exposures (weighted means of detections in all the 300s frames) in Table 1 to show the giant branches and as a check on the cleaning procedure. The original on-cluster data from all the exposures in Table 1 is shown in a color-magnitude diagram (CMD) in Figure 3a (2473 stars). The CMD for the “field” stars is shown in Figure 3b. Table 2 (given in its entirety in the electronic edition) lists the input data for the  $\omega$  Cen field, Table 3 gives the data for the off-cluster field, and Table 4 gives the data for NGC 6397.

To remove non-members from the cluster, we adapted a method used in Mighell, Sarajedini and French (1998), which also utilized statistical analysis from Gehrels (1986). We describe the method briefly here, but a detailed description is given in Appendix A. For each star in the  $\omega$  Cen field, we counted the number of stars in the CMD which have  $(b - y)$  and  $m_1$  colors within  $\max(2\sigma, 0.1)$  mag., and V-magnitudes within  $\max(2\sigma, 0.2)$  mag. of

the  $V$ ,  $(b-y)$  and  $m_1$  values for the “cluster” star. Then, we took the values of  $V$ ,  $(b-y)$  and  $m_1$  for each “cluster” star to the list of stars in the off-cluster field and obtained the number of field stars falling within the same limits, and calculated the probability that each star in the  $\omega$  Cen region was a member (for more details, see Mighell, Sarajedini and French 1998). Then, if a uniform random number generator gave a probability less than our calculated probability, the star was accepted as a cluster member. Figure 3c shows the accepted cluster members as open circles. The  $m_1$  vs.  $(b-y)$  color-color plot for the original  $\omega$  Cen sample is shown in Figure 3e, the off-cluster field stars are shown in Figure 3f, and the clean sample is shown in Figure 3g as open circles. The outliers in Figure 3g were examined; we decided that the cluster population had  $-0.2 < m_1 < 0.25$ . The final cleaned sample for  $\omega$  Cen (2121 stars) is seen as a CMD in Figure 3d, and a color-color plot in Figure 3h. Most objects on the giant branches are preserved and the far-outliers are removed.

We did not observe an off-cluster field for NGC 6397, and even though this cluster is in a much more field-contaminated region than  $\omega$  Cen (Anthony-Twarog, Twarog and Suntzeff 1992). We used the same off-cluster field to remove field stars from NGC 6397; obviously, the off-cluster field is at a different galactic latitude, but again we wanted to see if we could discriminate between a “contaminated” single-metallicity cluster and  $\omega$  Cen. Figure 4a shows the original sample from NGC 6397, Figure 4b shows the off-cluster field and Figure 4c the cleaned data. Examining the outliers in Figure 4g enabled us to select the final cleaned sample in the CMD in Figure 4d (747 stars) and color-color plot in Figure 4h. Because of the greater degree of field contamination, this sample will almost certainly have some non-members remaining although the restriction that  $-0.2 < m_1 < 0.15$  will have removed the majority of them.

Figure 5a shows the histogram of the  $m_1$ -index for  $\omega$  Cen, which has a mean of  $m_1 = 0.042 \pm 0.066$  (which is the dispersion in the distribution; considering the uncertainties

in the  $m_0$  data, intrinsic dispersion in  $m_0 = 0.06$ ). Figure 5b shows the data from Mukherjee *et al.* (1992) (unbroken line) and the same data shifted by 0.069 in  $m_1$  (dashed line, as they recommended, to fit the standard system). Our histogram is not significantly different in peak and shape, but we have a larger data set. The  $m_1$ -distribution for NGC 6397 is shown in Figure 5c, which has mean  $m_1 = 0.017 \pm 0.041$  (intrinsic dispersion in  $m_0 = 0.03$ ). So, the noisy data for the cluster with lower metallicity does appear more metal poor in  $m_1$  and has a distribution width about 60% that of  $\omega$  Cen (which is likely to be an artifact of the larger uncertainties in the NGC 6397 data set). The off-cluster field  $m_1$ -distribution is shown in Figure 5d.

#### 4. Analysis

We correct for the effect of interstellar reddening on the colors by adopting the relation of Crawford and Mandwewala (1976), with error estimated by Nissen (1981):

$$E(m_1) = -0.32E(b - y) \pm 0.03, \quad (13)$$

hence

$$m_0 = m_1 + 0.32E(b - y) \quad (14)$$

and

$$E(b - y) = 0.7E(B - V) \quad (15)$$

For  $\omega$  Centauri, we adopt  $E(B - V) = 0.15$ , giving  $E(b - y) = 0.105$ , with a distance modulus of  $(m - M) = 13.77$  (Dickens and Wooley 1967, which turns out to be close to the mean of the other studies). Other studies have used distance moduli ranging from 13.45 to 14.1 (De Marchi 1999, Bates *et al.* 1992, Mukherjee, Anthony-Twarog and Twarog 1992); we adopt the Dickens and Wooley distance, and a mean  $E(B - V)$  because they give the best fit to the most recent isochrones (VandenBerg *et al.* 1999). The uncertainty

in distance modulus of about 0.25 mag. renders an uncertainty in *absolute* age of 2-3 Gyr with a given set of isochrones (Bergbusch and Vandenberg 1997), but does not affect the *relative* ages derived for stars within  $\omega$  Cen. For NGC 6397, we adopt  $(m - M) = 12.13$  and  $E(B - V) = 0.185$  (Reid and Gizis 1998). Hence, for  $\omega$  Cen:

$$(b - y)_0 = (b - y) - 0.105 \quad (16)$$

and

$$m_0 = m_1 + 0.034 \quad (17)$$

Henceforth,  $m_0$  is the dereddened  $m_1$ -index.

## 5. The $m_1$ -Index

The  $m_1$ -index is very sensitive to the metallicity in stars of the color range of the giants, so we can use the metallicity to exclude a few stars whose metallicity is clearly outside the distribution.

We now select the objects in our  $\omega$  Cen data set around the MSTO. Apart from the well-studied relationship between the  $m_1$ -index and  $[\text{Fe}/\text{H}]$  for giants (Schuster and Nissen 1989, Grebel and Richtler 1992), we need a relationship to convert  $m_1$  to  $[\text{Fe}/\text{H}]$  for the upper main-sequence, the MSTO and the sub-giant branch. We use the work from Malyuto (1994), which gives similar results to Schuster and Nissen (1989), but is a more stable fit to the available data. Malyuto determined a relationship between  $m_1$  and  $[\text{Fe}/\text{H}]$  within the following ranges:

$$0.22 \leq (b - y) \leq 0.38 \quad (18)$$

$$0.03 \leq m_1 \leq 0.22 \quad (19)$$

$$-3.5 \leq [Fe/H] \leq 0.2 \quad (20)$$

Following Malyuto’s (1994) notation, we use:

$$(B - Y) = ((b - y) - 0.22)/0.16 + 1 \quad (21)$$

$$M_1 = (m_1 - 0.03)/0.19 + 1 \quad (22)$$

$$\begin{aligned} [Fe/H] = & 5.7071(B - Y)M_1 - 49.9162(B - Y)\log M_1 + 7.9971(B - Y)^2\log M_1 \\ & - 0.5895(B - Y)^3 - 24.0889(1/M_1) + 14.6747 \end{aligned} \quad (23)$$

Malyuto determined an uncertainty of  $\sigma_{[Fe/H]} = 0.15$ .

Grebel and Richtler’s (1992) calibration for giants is:

$$[Fe/H] = \frac{m_1 + a_1(b - y) + a_2}{a_3(b - y) + a_4} \quad (24)$$

where  $a_1 = -1.24 \pm 0.006$ ,  $a_2 = 0.294 \pm 0.03$ ,  $a_3 = 0.472 \pm 0.04$ ,  $a_4 = -0.118 \pm 0.02$ , and equations (18)-(24) imply *intrinsic* (unreddened) colors, which we diagram as  $m_0$ .

The loci of equal metallicities in the  $(b - y)$  vs. *metallicity* diagram are well approximated by straight lines within certain color ranges, but not  $0.26 \leq (b - y) \leq 0.36$  (the MSTO), which interests us. The straight-line approximation is valid for dwarfs for  $0.4 \leq (b - y) \leq 0.8$ . For giants and supergiants, the range is  $0.4 \leq (b - y) \leq 1.1$ . Grebel and Richtler (1992) show that there is no difference in the behavior of giants and supergiants. Figure 6 shows the 2121 stars in the “clean”  $\omega$  Cen sample, along with the straight-line fits to the giants from Grebel and Richtler (1992) and the heavy curves from the Malyuto (1994) calibrations for the MSTO stars.

Figure 7 shows a plot of  $m_0$  vs.  $[Fe/H]_{calc}$  from our data, using Equation (23), for the objects in the MSTO region of  $\omega$  Cen (Figure 7a) and NGC 6397 (Figure 7b). We chose the

objects at the MSTO in both clusters fitting the calibration ranges. It appears that about a quarter of the  $\omega$  Cen stars plotted in Figure 7a show a noticeably asymmetric scatter in  $m_0$ , away from the calibration line, indicating that for these stars, something other than  $[Fe/H]$  affects the  $m_0$ -index. In contrast, the NGC 6397 stars in Figure 7b appear well fitted by the Malyuto calibration. This effect on the metallicity index in  $\omega$  Cen has been noted before by Mukherjee *et al.* (1992) and was mentioned in Schuster and Nissen (1989). The former authors suggest that it is due to an enhancement of the CN-bands in the stars with relatively high  $m_0$  values. Even 47 Tuc, which shows no evidence of a metallicity spread, exhibits a spread in CN-strength extending to the MSTO (Briley, Hesser and Bell 1991). It seems surprising that moderately metal-poor stars should show an enhancement of a molecule consisting of two heavy elements since the concentration of such diatomics should depend on the square of the metallicity. However, it is distinctly possible that the atmospheres of stars near the  $\omega$  Cen MSTO could be polluted by the ejecta of Wolf-Rayet stars, which are greatly enhanced in C and N, but not with the heavier species. If  $\omega$  Cen was able to retain the ejecta from supernovae (Morgan and Lake 1989), then the ejecta from Wolf-Rayet stars should also be retained. This effect could explain the 47 Tuc observations, where the cluster was not massive enough to retain supernovae ejecta.

It is known that  $\omega$  Cen has CN-abundance anomalies amongst its giants (Suntzeff and Kraft 1996, Norris and DaCosta 1995), which can affect the metallicity index; the presence of the CN-band extending to the violet from 4216Å reduces the flux in the  $v$ -band and pushes the  $m_1$ -index higher, which does not mean that the overall metallicity has changed (Richter *et al.* 1999, Anthony-Twarog *et al.* 1995). As stated above, 47 Tuc, which doesn't appear to have a dispersion in  $[Fe/H]$  on the giant branch, shows CN-variations at the MSTO, which is thought to be a surface-contamination effect (Cannon *et al.* 1998).

To avoid selecting stars which may not have a simple calibration of  $m_0$  to metallicity,

we excluded the stars falling away from the calibration line in Figure 7. This process also excludes most binaries. The 739 objects which met our selection criteria are shown as filled circles in Figure 7a (rejected objects are shown as open circles). In NGC 6397, 462 stars passed the selection criteria (Figure 7b). In NGC 6397, which is not known to have anomalous abundances (Anthony-Twarog, Twarog and Suntzeff 1992), the scatter is probably due to a larger  $\sigma_{m_0}$ , binarity and/or overlapping PSFs.

## 6. Discussion and Conclusions

### 6.1. The Age-Metallicity Relation

We want to look for an age spread at the MSTO in addition to  $\omega$  Cen’s metallicity spread, so we must take care to disentangle the effects of age and chemical composition. By removing stars from our samples which did not fit the calibration equation, we should have removed the effect of anomalous abundances and multiple sources (Schuster *et al.* 1996). Figure 8 shows the 10 Gyr isochrones for a range in metallicities as modeled by VandenBerg *et al.* (1999). *If stars are all the same age, the redder objects should have a higher metallicity.*

First, we compare the  $\omega$  Cen stars to the isochrones corresponding to the mean (spectroscopic) metallicity,  $[Fe/H] = -1.54$  in Figure 9. These isochrones are the best fit to the upper main-sequence and MSTO, but are not a good fit to the subgiants. This is a consequence of using the Kurucz (1992) colors as a conversion, tied to the MSTO region (VandenBerg: private communication). We were encouraged that the latest  $\alpha$ -enhanced isochrones suggested a lower age for both clusters, in line with the new *Hipparcos* results (Reid 1997). In Figure 9, we now divide the selected MSTO sample into three metallicity groups: Figure 9a shows relatively high-metallicity objects:  $-1.2 < [Fe/H] < -0.5$  (filled

triangles), Figure 9b shows the medium-metallicity group:  $-1.6 < [Fe/H] < -1.2$  (open squares), and the low-metallicity stars are shown in Figure 9c:  $-2.2 < [Fe/H] < -1.6$  (open circles). ( $\sigma_V = \sigma_{b-y} \leq 0.01$ , and  $\sigma_{m_1} \leq 0.015$ ). Clearly, the relatively metal-rich group (filled triangles) in Figure 9a appear younger than the metal-poor group (if we assume the whole population is described by the  $[Fe/H] = -1.54$  isochrones. In this example, the group with  $-1.2 < [Fe/H] < -0.5$  has a mean age of  $9.7 \pm 1.8$  Gyr; the  $-1.6 < [Fe/H] < -1.2$  group has a mean age of  $10.2 \pm 1.3$  Gyr; and the  $-2.2 < [Fe/H] < -1.6$  has a mean age of  $11.1 \pm 1.2$  Gyr. So, in this case the age range would be about 1.4 Gyr, with the metal-content increasing towards younger stars (as one would expect with self-enrichment). The NGC 6397 stars are all consistent with being the same age, we find the mean for the whole NGC 6397 sample is  $12.0 \pm 0.7$  Gyr; any decrease of age with increasing metal-content is hidden by the uncertainties.

Now, we examine the relatively high-, medium- and low-metallicity groups in  $\omega$  Cen with isochrones of *different* metallicities, corresponding to  $\sim$  the mean  $[Fe/H]$  within each group (Figures 9a–c). The isochrones in Figure 10a, which contains the most metal-rich stars, are not a good fit to the data but indicate an age of about 8 Gyr for the stars with the best photometry. Figure 10b shows the mid-range group to have a mean age of  $9.4 \pm 1.4$  Gyr, and Figure 10c shows the low-metallicity group to have a mean age of  $12.7 \pm 1.5$  Gyr. So, Figure 10 implies that there is a 2–4 Gyr age range in  $\omega$  Cen. From Figure 5, there is no strong evidence of a bimodal metallicity distribution from the  $m_1$ -index. This may be a CN-abundance effect which is gradually reduced as the stars undergo mixing during later evolution (discussed in Cannon *et al.* 1998).

Figure 11a, b and c show the NGC 6397 stars selected in the same way as the  $\omega$  Cen stars in Figures 9 and 10, with the isochrones corresponding to a metallicity of  $[Fe/H] = -1.84$ . These stars are not well-described by any other set of isochrones,



and there are few stars with good photometry ( $\sigma_V = \sigma_{b-y} \leq 0.012$ , and  $\sigma_{m_1} \leq 0.023$ ) in the apparently high-metallicity group (Figure 11a), as we expect from a cluster with mostly metal-poor stars. Most of the scatter in Figure 11 is caused by the photometric uncertainties, and the cluster stars appear to be just under 12 Gyr-old on this set of isochrones.

In order to explore the relationship between age and metallicity (if any), we split the stars in both clusters into narrow ranges in apparent metallicity:  $[Fe/H] = -1.0 \pm 0.1; -1.15 \pm 0.1; -1.3 \pm 0.1; -1.4 \pm 0.1; -1.55 \pm 0.1; -1.6 \pm 0.1; -1.7 \pm 0.1; -1.82 \pm 0.08; -2.0 \pm 0.1; -2.15 \pm 0.1$ . We examined the distribution of mean age with calculated  $[Fe/H]$  for  $\omega$  Cen (Figure 12a), and NGC 6397 (Figure 12b). The latter cluster’s stars can only be fit well using the isochrones corresponding to the mean metallicity  $[Fe/H] = -1.84$ . The age spread implied by Figure 12a is at least 3 Gyr and could be as much as 4 Gyr for  $\omega$  Cen. NGC 6397 shows no obvious trend of age with metallicity within the uncertainties, with the stars having a weighted mean age of 12 Gyr (dominated by points with the smallest error bars). NGC 6397 is more metal-poor than  $\omega$  Cen, as expected, and is described by a single-metallicity and a single age.  $\omega$  Cen appears to have a mixture of relatively old metal-poor stars and a younger metal-rich population, although some of these stars could have suffered surface contamination.

## 6.2. Possible Histories of $\omega$ Cen

We have found that there is an age range of at least 3 Gyr in  $\omega$  Cen, and that the stars with higher metallicity are younger; this evidence supports the self-enrichment theory. Hilker and Richtler (1999) have found that Strömgren photometric observations of 1400 red giants show that the age spread between the metal-poor and metal-rich stars is about 3 Gyrs, with the latter also being younger. Hence the age spread holds for both the evolved

and unevolved stars.

We now look into the origin of the observed age-metallicity correlation. Three possibilities were mentioned in the Introduction:

1. A chemically diverse parent cloud;
2. A merger of two clusters;
3. Self-enrichment within a single entity.

We can easily eliminate the first possibility. While a chemically diverse parent cloud – one in which the dust-to-gas ratio varies within the cloud – could account for the metallicity spread, there is no reason for such a model to yield an age-metallicity relation. The possibility that  $\omega$  Cen is a merger has been suggested by Norris *et al.* (1997) on the basis of a second peak in the metallicity distribution and an apparent difference in the kinematics of the metal-poor and metal-rich stars. The wide spread in metallicity, confirmed by Norris and Da Costa (1995) indicates that both of the merging clusters must have had an original metallicity spread. In addition the correlation of s-process elements with metallicity, reaching  $[s/Fe] = 1.0$  at  $[Fe/H] = -1.3$  and  $[s/Fe] = 1.5$  at  $[Fe/H] = -0.7$  shows that the chemical history of  $\omega$  Cen (or its two progenitor clusters) has been different from that in any other globular cluster in the Galaxy so far analyzed (Vanture *et al.* 1994). In other words, both the metal-poor and the metal-rich clusters behaved in a very unusual way with regard to their s-process enrichment. These considerations point to self-enrichment in a single object.

In discussing self-enrichment in globular clusters, Morgan and Lake (1989) require that 330 supernovae of type II must have provided  $\omega$  Cen with  $165M_{\odot}$  of iron. The mass limit needed to contain the supernovae and retain the ejecta was calculated to be  $2.9 \times 10^6 M_{\odot}$ , which is close to the total mass of the cluster today. Morgan and Lake’s calculations

suggest that the primordial cloud from which  $\omega$  Cen formed did not have to be 10-100 times as massive (Padoan, Jiminez and Jones 1997). Having the star formation continue for a free-fall time ( $10^7$  years) all over the cloud to enrich its gas with iron would reduce the time of star formation well below the level of detectability.

To enrich the cluster in s-process elements  $\omega$  Cen needed time to form stars of  $2-8M_{\odot}$  which then dumped enriched material into the cluster’s interstellar gas during their AGB phase. This process should have taken about a billion years and must have been completed before the more powerful Type Ia supernovae, or a collision with a Galactic gas cloud, swept out the rest of the gas from the cluster. It seems that the greater mass of  $\omega$  Cen, as compared with other globulars in our Galaxy was able to retain the enriched gas long enough to prolong the star formation process. Our data suggest that the oldest, metal-poor, stars are at least 3 Gyrs older than the youngest, metal-rich, stars. In contrast to other globular clusters, star formation in  $\omega$  Cen must have survived the formation and explosion of the first massive stars (on a time-scale of  $10^6$  to  $10^7$  years) which should have expelled the gas from less massive globulars.

For how long did SNIIs continue to contribute metals to  $\omega$  Cen? The abundances of Norris and Da Costa (1995) show that the  $\alpha$ -elements; Mg, Si, Ca, and Ti, are enhanced with respect to iron all the way from  $[Fe/H] = -2.0$  to  $[Fe/H] = -0.7$ . Since a high  $[\alpha/Fe]$  ratio is associated with SNIIs, the supernovae were still contributing all these species while the s-process elements were building up from the contributions of  $2-8M_{\odot}$  stars. It appears that SNIas never contributed much iron to the cluster or else the value of  $[\alpha/Fe]$  would have diminished as  $[Fe/H]$  approached its maximum value. either the cluster was swept clean by the first SNIas or it lost its interstellar matter with Galactic gas clouds about when  $[Fe/H]$  reached -0.7.

In agreement with Suntzeff and Kraft (1996), we find no strong evidence of bimodality

in the distribution of the  $m_1$ -index, but there is some evidence in the plot of age vs. metallicity. This evidence alone cannot rule between the merger of formed clusters or two bursts of star formation; also, the evidence does not rule out the accretion of another proto-globular cloud into  $\omega$  Cen early in its history (Norris *et al.* 1997). The fact that  $\omega$  Cen did not lose its interstellar matter through interaction with Galactic gas clouds for several billion years is difficult to imagine if it has always been in its present orbit (Dinescu *et al.* 1999). The only way that it could have avoided doing so was to be in an orbit far from the plane of the Milky Way. If this was so,  $\omega$  Cen must have been a satellite galaxy (or the nucleus of a galaxy) that was captured about 8 Gyrs ago. This possibility has also been suggested by Dinescu *et al.* and by Majewski *et al.* (1999).

We would like to thank Guillermo Gonzalez, Ken Mighell, John Norris, Peter Stetson, Don VandenBerg, George Lake and Barbara Anthony-Twarog for useful discussions, and the support staff at CTIO for extra help in dealing with large-format images.

## A. “Cleaning” the Cluster

This method of “cleaning” the cluster membership has been adapted from Mighell, Sarajedini and French (1998). Since we have separate images of the on-cluster and off-cluster fields, our use of this method is more straightforward than their formalism. In addition, instead of having a CMD ( $V$ ,  $(b - y)$ , Figure 3a) alone, we also have a color-color plot ( $m_1$ ,  $(b - y)$ , Figure 3e). For each star in the on-cluster field CMD (Figure 3a), we count the number of stars in the CMD which have  $V$ -magnitudes within  $\max(2\sigma, 0.2)$  mag., and  $(b - y)$  and  $m_1$  colors. We call this number  $N_{on}$ . Now, we also count the number of *field* stars, in the off-cluster image, which fall within the same ranges in  $V$ ,  $(b - y)$ , (Figure 3b) and  $m_1$  (Figure 3f), that were determined for the star in the *cluster* field. We call this

number  $N_{off}$ . We calculate the probability that the star in the on-cluster field CMD is a member of the globular cluster population as:

$$p \approx 1 - \min \left( \frac{\alpha N_{off}^{UL\ 84}}{N_{on}^{LL\ 95}}, 1.0 \right) \quad (A1)$$

where  $\alpha$  is the ratio of the area of the cluster region to the area of the field region, and

$$N_{off}^{UL\ 84} \approx (N_{off} + 1) \left[ 1 - \frac{1}{9(N_{off} + 1)} + \frac{1.000}{3\sqrt{N_{off} + 1}} \right]^3 \quad (A2)$$

(corresponding to eq.(2) of Mighell, Sarajedini and French 1998, and eq.(9) of Gehrels 1986), is the estimated upper ( $\sim 84\%$ ) confidence limit of  $N_{off}$ , using Gaussian statistics.

Now,

$$N_{on}^{LL\ 95} \approx N_{on} \times \left[ 1 - \frac{1}{9N_{on}} - \frac{1.645}{3\sqrt{N_{on}}} + 0.031N_{on}^{-2.50} \right]^3 \quad (A3)$$

is the lower 95% confidence limit for  $N_{on}$  (eq.(3) of Mighell, Sarajedini and French 1998, and eq.(14) of Gehrels 1986). For  $\omega$  Cen, we assume that the whole on-cluster field is part of  $\omega$  Cen (a fairly safe assumption), so that  $\alpha$  is assumed to be  $\sim 1$ , in this case.

To estimate if any particular star is a cluster member, we generate a uniform random number,  $0 \leq p' \leq 1$ , and if  $p' \leq p$ , we accept the star as a member of the cluster. The cleaned cluster stars for  $\omega$  Cen are shown as a CMD (2154 objects) in Figure 3c and as a color-color plot in Figure 3g. This is a probabilistic method, so the resulting CMD has to be considered to be “one of an infinite number of different possible realizations” (Mighell, Sarajedini and French 1998) of the cleaned cluster population. Few field stars are found in the MSTO region of the CMD, whereas many contaminate the region of the giant branches; therefore the MSTO may be undercleaned and the evolved stars may be overcleaned. We considered the color-color plot in Figure 3g, carefully looking at the positions of the outlying stars. We consider the cluster sequences to lie between  $-0.2 < m_1 < 0.25$ , rejecting 33 additional objects, but preserving the horizontal branch and possible blue stragglers.

## REFERENCES

- Alcaino, G., Liller, W., Alvarado, F., Kravtsov, V., Ipatov, A., Samus, N., & Smirnov, O. 1997 AJ, 114, 1067.
- Alcaino, G., & Liller, W. 1987, AJ, 94, 1585
- Anthony-Twarog, B.J., & Twarog, B.A. 1994, AJ, 107, 1577.
- Anthony-Twarog, B.J., Twarog, B.A., & Craig, J. 1993, PASP, 107, 32.
- Anthony-Twarog, B.J., Twarog, B.A., & Suntzeff, N.B. 1992, AJ, 103, 1264.
- Astronomer Royal, Royal Observatory Annals, *Number 2*, “Studies of the Globular Cluster  $\omega$  Cen I. Catalogue of Magnitudes and Proper Motions,” 1966, London: Her Majesty’s Stationary Office.
- Bates, B., Wood, K.D., Catney, M.G., & Gilheany, S. 1992, MNRAS, 254, 221.
- Bergbusch, P.A., & Vandenberg, D.A. 1992, ApJS, 81, 163.
- Bergbusch, P.A., & Vandenberg, D.A. 1997, AJ, 114, 2604.
- Briley, M.M., Hesser, J.E., & Bell, R.A. 1991, ApJ, 373, 482.
- Brown, J.H., Burkert, A., Truran, J.W., 1991, ApJ, 376, 115. 249, L13.
- Brown, J.A., Wallerstein, G., & Oke, J.B. 1990 AJ, 100, 1561.
- Butler, D., Dickens, R.J., & Epps, E. 1978, ApJ, 225, 148.
- Cannon, R.D., Croke, B.F.W., Bell, R.A., Hesser, J.E., & Stathakis, R.A. 1998, MNRAS, 298, 601.
- Crawford, D.L., and Mandwewala, N. 1976, PASP, 88, 917.
- De Marchi, G. 1999, AJ, 117, 303.
- Dickens, R.J., & Wooley, R. 1967, Royal Observatory bulletins. Series E; no.128, London:H.M.S.O., p.255.

- Dinescu, D.I., Girard, T.M., van Altena, W.F. 1999, AJ, 117, 1792.
- Freeman, K.C. 1993, in A.S.P. Conf. Ser. Vol. 48, “*The Globular Cluster-Galaxy Connection*,” Edited by G.H.Smith & J.P.Brodie, p.27.
- Folgheraiter, E.L., Penny, A.J., Griffiths, W.K., & Dickens, R.J. 1995, MNRAS, 274, 407.
- Gehrels, N. 1986, ApJ, 303, 336.
- Gratton, R.G., Fusi Pecci, F., Carretta, E., Clementini, G., Corsi, C.E., & Lattanzi, M. 1997, ApJ, 491, 749.
- Grebel, E. K., & Richtler, T. 1992 A&A, 253, 359.
- Hilker, M., & Richtler, T. 1999, A&A, , in *Proceedings of the 35th Liege International Astrophysics Colloquium: “The Galactic Halo: from Globular Clusters to Field Stars*, in press (astro-ph/9910370).
- Kilkenny, D., & Laing, J.D. 1992, MNRAS, 225, 308.
- Kurucz, R.L. 1992, Kurucz CD-ROM 19, Solar Abundance Model Atmospheres (Cambridge: SAO).
- Evans, T.L. 1983, MNRAS, 204, 975.
- Majewski, S.R., Patterson, R.J., Dinescu, D.I., Johnson, W.Y., Ostheimer, J.C., Kunkel, W.E., Palma, C. 1999, in *Proceedings of the 35th Liege International Astrophysics Colloquium: “The Galactic Halo: from Globular Clusters to Field Stars*, in press (astro-ph/9910278).
- Malyuto, V. 1994, A&AS, 108, 441.
- Mighell, K.J., Sarajedini, A., & French, R.S. 1998, AJ, 116, 2395.
- Morgan, S. & Lake, G. 1989, ApJ, 339, 171.
- Mukherjee, K., Anthony-Twarog, B.J., & Twarog, B.A. 1992, PASP 104, 561.

- Nissen, P.E. 1981, *A&A*, 97, 145.
- Norris, J.E., & Da Costa, G.S. 1995, *ApJ*, 447 680.
- Norris, J.E., Freeman, K.C., & Mighell, K.J. 1996, *ApJ*, 462, 241.
- Norris, J.E., Freeman, K.E., Mayor, M. & Seitzer, P. 1997, *ApJ*, 487, 187.
- Padoan, P., Jimenez, R, & Jones, B. 1997 *MNRAS*, 185, 711.
- Parmentier, G., Jehin, E., Magain, P., Neuforge, C., Noels, A. & Thoul, A.A. 1999, *A&A*,  
in press (astro-ph/9911258).
- Reid, N.I. 1997, *AJ*, 114, 161.
- Reid, N.I., & Gizis, J.E. 1998, *AJ*, 116, 2929.
- Richter, P., Hilker, M., & Richtler, T. 1999, *A&A*, in press (astro-ph/9907200).
- Schuster, W.J., & Nissen, P.E. 1989, *A&A*, 222, 69.
- Schuster, W.J., Nissen, P.E., Parrao, L., Beers, T.C., & Overgaard, L.P. 1996, *A&AS*, 117,  
317.
- Stetson, P.B., Davis, L.E., & Crabtree, D.R. 1990, in *CCDs in Astronomy*, ASP Conf. Ser.  
8, 289, Ed. G.H. Jacoby.
- Strömgren, B. 1966, *ARAA*, 4, 433.
- Suntzeff, N.B. & Kraft, R.P. 1996, *AJ*, 111, 1913.
- VandenBerg, D.A., & Bell, R.A. 1985, *ApJS*, 58, 561.
- VandenBerg, D.A., Swenson, F.J., Rogers, F.J., Iglesias, C.A., & Alexander, D.R. 1999, in  
preparation.
- Van den Bergh, S. 1993, *ApJ*, 411, 178.
- Vanture, A.D., Wallerstein, G., & Brown, J.A. 1994, *PASP* 106, 835.
- Wood, K.D., & Bates, B. 1994, *MNRAS*, 267, 660.



Wood, K.D., & Bates, B. 1993, ApJ, 417, 572.

## Figure Captions

**Figure 1:** A  $12.5 \times 12.5$  arcminute Strömgren y-frame of a field north of the center of  $\omega$  Centauri with a 1500-second integration time. The field center is at  $\alpha = 13^h 26^m 46.0^s$  and  $\delta = -47^\circ 15' 00''$ , which contains the field used for Eggen’s photoelectric sequence (*Astronomer Royal*, ROA #2, 1996) Number 2, (1966). The frame has been oriented so that north is at the top and east is to the left.

**Figure 2:** Left panels: all objects in the  $\omega$  Cen field with a detection at any 3 vby frames (10981 sources) on 05/10/96 (from y:  $3 \times 900s$  &  $1 \times 1500s$ , b:  $3 \times 900s$  &  $1 \times 1800s$ , and v:  $3 \times 900s$  &  $1 \times 2000s$ , see Table 1): **a:** Uncertainty in the  $m_1$ -index vs. V magnitude. **b:** Uncertainty in the  $(b - y)$ -index vs. V magnitude. **c:** Uncertainty in the  $V$ -magnitude vs. V magnitude. Right panels: objects detected in *all* the above frames (2147 objects) on 05/10/96 (see Table 1) with the V,  $(b - y)$  and  $(v - b)$  values calculated as the weighted mean of multiple detections: **d:** Uncertainty in the  $m_1$ -index vs. V magnitude. **e:** Uncertainty in the  $(b - y)$ -index vs. V magnitude. **f:** Uncertainty in the  $V$ -magnitude vs. V magnitude.

**Figure 3:** **a:** 2473 objects in  $\omega$  Cen (2147 from the longer frames in Table 1 plus the weighted-mean data from the 300-second exposures, tracing the giant branches). **b:** 536 objects from the off-cluster field. **c:** 2154 objects after the first cleaning process shown as open circles. **d:** 2121 objects in the final sample after limiting the  $m_1$ -index to  $-0.2 < m_1 < 0.25$ . **e:**  $m_1$  vs.  $(b - y)$  color-color diagram for the original 2473 objects in the  $\omega$  Cen field. The straight-line fits are for the giants, taken from Grebel and Richtler (1992). **f:**  $m_1$  vs.  $(b - y)$  color-color diagram for the off-cluster field containing 536 sources. **g:**  $m_1$  vs.  $(b - y)$  color-color diagram for the 2154 stars in  $\omega$  Cen after the first cleaning pass. **h:**  $m_1$  vs.  $(b - y)$  color-color diagram for the 2121 stars in  $\omega$  Cen after rejecting the far outliers, which preserves the horizontal branch and possible blue stragglers. Stars with very low  $m_1$  may have colors affected by an unseen hot companion.

**Figure 4:** **a:** 976 objects in NGC 6397 from the  $3 \times 600s$  exposures at y, and the 900s exposures at b and v. **b:** 536 objects from the off-cluster field (same field as used for  $\omega$  Cen to test the cleaning procedure). **c:** 808 objects after the first cleaning process shown as open circles. **d:** 747 objects in the final sample after considering limits on the  $m_1$ -index. **e:**  $m_1$  vs.  $(b - y)$  color-color diagram for the original 976 objects in the NGC 6397 field. The straight-line fits are the loci of equal-metallicity giants from Grebel and Richtler (1992). **f:**  $m_1$  vs.  $(b - y)$  color-color diagram for the off-cluster field containing 536 sources. **g:**  $m_1$  vs.  $(b - y)$  color-color diagram for the 808 sources after the first cleaning pass. **h:**  $m_1$  vs.  $(b - y)$  color-color diagram for the 747  $\omega$  Cen stars after rejecting the outliers in **f**.

**Figure 5:** **a:** Histogram of the  $m_1$ -index for the 2121 objects in the cleaned  $\omega$  Cen sample. The sample mean is  $m_1 = 0.042 \pm 0.066$ , and we fit a gaussian to the histogram with those parameters. **b:** Histogram of the  $m_1$ -index for the Mukherjee *et al.* (1992) sample (solid line) and shifted by their recommended correction (dashed line). The histogram of shifted data is not significantly different in shape from our sample (apart from their truncation in  $m_1$ ), but we have a larger sample of objects. **c:** Histogram of the  $m_1$ -index for the 747 objects in NGC 6397. The cluster mean is  $m_1 = 0.017 \pm 0.041$ . **d:** Histogram of the  $m_1$ -index for the 536 objects in the off-cluster field.

**Figure 6:**  $m_0$  vs.  $(b - y)_0$  color-color diagram for the 2121 stars in the final clean  $\omega$  Cen sample. We show the Grebel and Richtler (1992) metallicity calibration lines (a straight-line approximation) for giants, and the Malyuto calibration curves (heavy lines) for the MSTO stars.

**Figure 7:** **a:** Plot of reddening-free metallicity index,  $m_0$  in  $\omega$  Cen, against the calculated metallicity from Malyuto (1994) for the ranges:  $0.22 \leq (b - y) \leq 0.38$ ;  $0.03 \leq m_1 \leq 0.22$ ;  $-3.5 \leq [Fe/H] \leq 0.2$ . (We use the Malyuto (1994) calibration from Equation (23), but the Schuster and Nissen (1989) calibration does not make a great

difference to the calculated  $[\text{Fe}/\text{H}]$  values). There were 1124 sources in  $\omega$  Cen within this range and the filled circles are the objects (853) which are a good fit to the calibration line. The open circles are sources which fell in the correct color range, but were not a good fit. Reasons for some stars not being well-fit by the calibration could be anomalous  $m_0$ -values owing to enhanced CN-abundance, strong G-bands, measurement errors or binarity/merged images (Schuster *et al.* 1996). The scatter is most pronounced at the high-metallicity end, supporting the idea some kind of CN-enhancement is probably responsible. **b:** Plot of reddening-free metallicity index,  $m_0$  in NGC 6397, against the calculated metallicity from Malyuto (1994). There were 541 within the Malyuto (1994) calibration range and 462 were good fits to the line. As we expect, there is less scatter in this plot because NGC 6397 is not known to have abundance anomalies. The outliers are most likely caused by binarity and merged images here, so this method is a way to remove these objects from the sample; the true binary fraction in NGC 6397 could be around 10% (Alcaino *et al.* 1997), while it is considered to be lower in  $\omega$  Cen (Mukherjee *et al.* 1992).

**Figure 8:** Color-magnitude diagram showing the effect of varying the input metallicity on the color of the main-sequence turn-off. We show the 10 Gyr isochrones for various metallicities from Vandenberg *et al.* (1999). If stars are the same age, the redder objects should be more metal-rich.

**Figure 9:** Color-magnitude diagrams of the main-sequence turn-off region of  $\omega$  Cen, shown with the isochrones with  $[\text{Fe}/\text{H}] = -1.54$ . We show the stars divided into groups of relatively high, medium and low metallicity. All objects shown as filled triangles, open squares and open circles have  $\sigma_V = \sigma_{b-y} \leq 0.01$ , and  $\sigma_{m_1} \leq 0.02$ . **a:** filled triangles have  $-1.2 < [\text{Fe}/\text{H}] < -0.5$ , and have a mean age of  $9.7 \pm 1.8$  Gyr; **b:** open squares have  $-1.6 < [\text{Fe}/\text{H}] < -1.2$ , and have a mean age of  $10.2 \pm 1.3$  Gyr; **c:** open circles have  $-2.2 < [\text{Fe}/\text{H}] < -1.6$ , and have a mean age of  $11.1 \pm 1.2$  Gyr. So, if all the stars are

well-fit by this set of isochrones, the stars which are relatively more metal-rich are younger than the more metal-poor stars, as you would expect from self-enrichment. To show where the MSTO and subgiant branch stars lie, all objects from the “cleaned” sample within the  $[Fe/H]_{calc}$  range with no restriction on colors or uncertainties are shown as tiny circles.

**Figure 10:** Color-magnitude diagrams of the main-sequence turn-off region of  $\omega$  Cen, shown with isochrones corresponding to the mean  $[Fe/H]_{calc}$  of that group. All stars shown as filled triangles, open squares and open circles have  $\sigma_V = \sigma_{b-y} \leq 0.01$ , and  $\sigma_{m_1} \leq 0.02$ . **a:** filled triangles have  $-1.2 < [Fe/H] < -0.5$ , isochrones correspond to  $[Fe/H] = -1.14$ , mean age  $< 8$  Gyr; **b:** open squares have  $-1.6 < [Fe/H] < -1.2$ , isochrones correspond to  $[Fe/H] = -1.41$ , mean age  $9.4 \pm 1.4$  Gyr; **c:** open circles have  $-2.2 < [Fe/H] < -1.6$ , isochrones correspond to  $[Fe/H] = -1.84$ , mean age  $12.7 \pm 1.5$  Gyr. To show where the MSTO and subgiant branch stars lie, all objects from the “cleaned” sample within the  $[Fe/H]_{calc}$  range with no restriction on colors or uncertainties are shown as tiny circles.

**Figure 11:** Color-magnitude diagrams of the main-sequence turn-off region of NGC 6397, shown with isochrones corresponding to the mean  $[Fe/H]_{calc}$  of the cluster,  $[Fe/H] = -1.84$ . All stars shown as filled triangles, open squares and open circles have  $\sigma_V = \sigma_{b-y} \leq 0.012$ , and  $\sigma_{m_1} \leq 0.023$ . **a:** filled triangles have  $-1.2 < [Fe/H] < -0.5$ , isochrones correspond to  $[Fe/H] = -1.84$ , there are few objects within the calibration range with very good photometry here, as we expected; **b:** open squares have  $-1.6 < [Fe/H] < -1.2$ , isochrones correspond to  $[Fe/H] = -1.84$ , consistent with a mean age of around  $11.7 \pm 0.9$  Gyr; **c:** open circles have  $-2.2 < [Fe/H] < -1.6$ , isochrones correspond to  $[Fe/H] = -1.84$ , mean age  $11.8 \pm 1.4$  Gyr. To show where the MSTO and subgiant branch stars lie, all objects from the “cleaned” sample within the  $[Fe/H]_{calc}$  range with no restriction on colors or uncertainties are shown as tiny circles.

**Figure 12:** Age spreads and metallicity spreads in the two clusters. **a:** Plot of

mean age against calculated  $[\text{Fe}/\text{H}]$  for  $\omega$  Cen. We divided the samples into groups with calculated  $[Fe/H] = -1.0 \pm 0.1; -1.15 \pm 0.1; -1.3 \pm 0.1; -1.4 \pm 0.1; -1.55 \pm 0.1; -1.6 \pm 0.1; -1.7 \pm 0.1; -1.82 \pm 0.1; -2.0 \pm 0.1; -2.15 \pm 0.1$ . We plotted these groups (with a narrow metallicity range) on a CMD. We estimated the age of each star individually from the VandenBerg *et al.* (1999) grid of isochrones corresponding to the mean metallicity of that group, between  $3 < M_V < 4$  mag. (where the isochrones are almost vertical). *Here, we see that the age spread in  $\omega$  Cen is 2–4 Gyr.* Uncertainties in  $[\text{Fe}/\text{H}]$  are estimated from the Malyuto calibration to be  $\sim \pm 0.15$ , and the uncertainty in the age is the standard deviation of the mean age within each metallicity group. **b:** Plot of mean age against calculated  $[\text{Fe}/\text{H}]$  for NGC 6397. We divided the samples into groups with calculated  $[Fe/H] = -1.0 \pm 0.1; -1.15 \pm 0.1; -1.3 \pm 0.1; -1.4 \pm 0.1; -1.55 \pm 0.1; -1.6 \pm 0.1; -1.7 \pm 0.1; -1.82 \pm 0.1; -2.0 \pm 0.1; -2.15 \pm 0.1$ . We plotted these groups (with a narrow metallicity range) on a CMD. We estimated the age of each star individually from the VandenBerg *et al.* (1999) grid of isochrones for  $[Fe/H] = -1.84$ , between  $3 < M_V < 4$  mag. (where the isochrones are almost vertical). NGC 6397 stars can only be fit by the average-metallicity isochrones. We see that there is no strong evidence that the metal-poor stars are older than the metal-rich stars, and the sample of stars here have a weighted mean age of  $11.7 \pm 0.1$  Gyr. The unweighted mean for the whole sample is  $12.0 \pm 0.7$  Gyr.

## Table Captions

**Table 1:** CTIO 0.9-m CCD Frames.

**Table 2:** Sample of Objects in  $\omega$  Cen.

**Table 3:** Objects in the Off-Cluster Field.

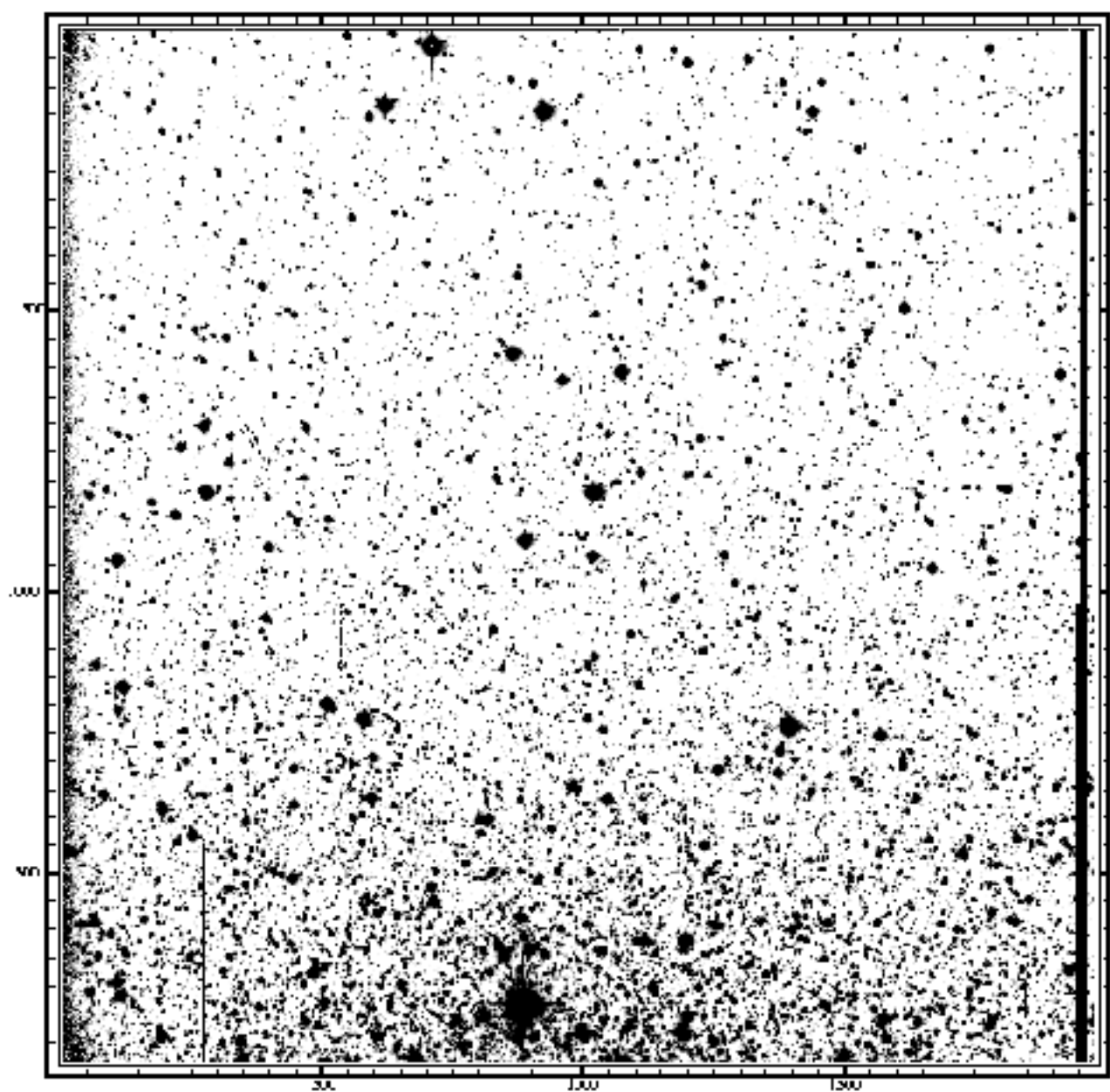
**Table 4:** Sample of Objects in NGC 6397.

Table 1. CTIO 0.9-m CCD Frames

Date	Field	Filter	Exposure(s)	Airmass <sup>1</sup>	FWHM(arcsec) <sup>2</sup>
05/09/96	Omega Cen N	y	5x300	1.136	1.4
"	13 <sup>h</sup> 26 <sup>m</sup> 46.0 <sup>s</sup> – 47°15′00″	b	5x300	1.193	1.4
"	"	v	5x300	1.263	1.5
05/10/96	Omega Cen N	y	3x900	1.179	1.8
"	13 <sup>h</sup> 20 <sup>m</sup> 46.0 <sup>s</sup> – 47°28′34″	b	3x900	1.100	1.7
"	"	v	3x900	1.058	2.0
"	"	y	1500	1.130	1.4
"	"	b	1800	1.177	1.5
"	"	v	2000	1.252	1.6
"	Off Cluster	y	300	1.485	2.1
"	"	b	300	1.513	2.2
"	"	v	300	1.547	2.3
"	"	y	900	1.584	2.0
"	"	b	900	1.686	2.1
"	"	v	900	1.804	1.8
05/12/96	NGC 6397	b	900	1.176	1.3
"	17 <sup>h</sup> 40 <sup>m</sup> 52.1 <sup>s</sup> – 53°40′32″	v	900	1.157	1.3
05/14/96	"	y	3x600	1.096	1.1

Note. — (1) Effective airmass for multiple exposures. (2) Average seeing for multiple exposures.





$z = 1-2$ ,  $2.00 \pm 0.004$  arcmin-linear Cor-2.65 Dc-0.52 comp-Galaxy mask noise ea-300

210 295 370 446 521 594

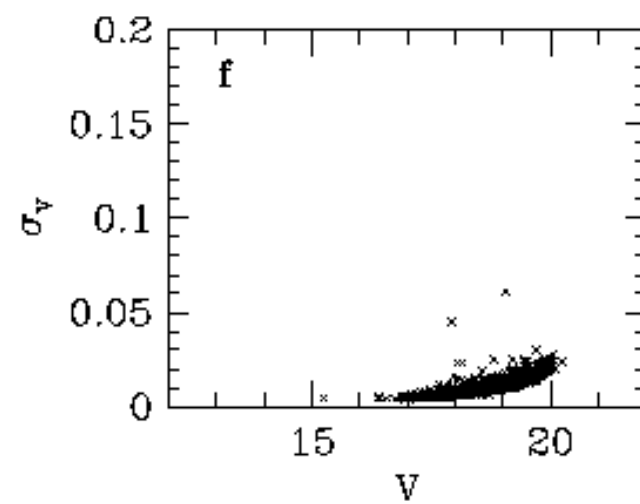
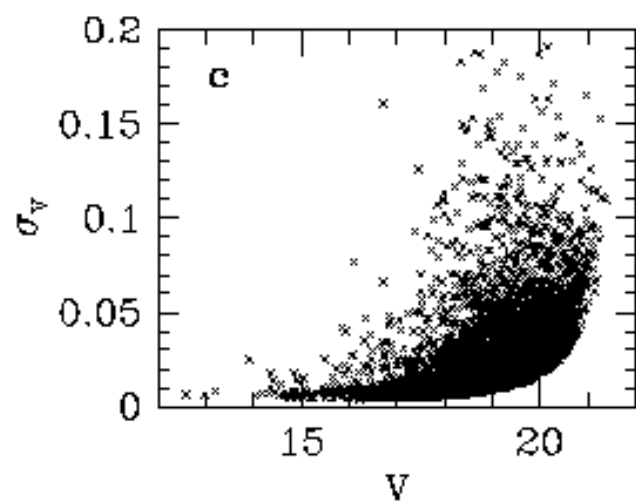
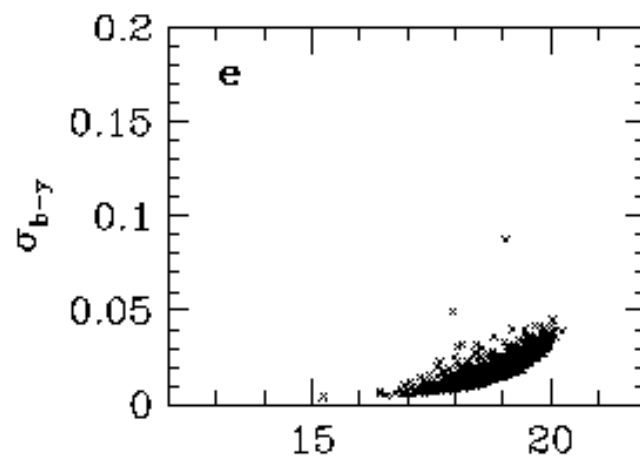
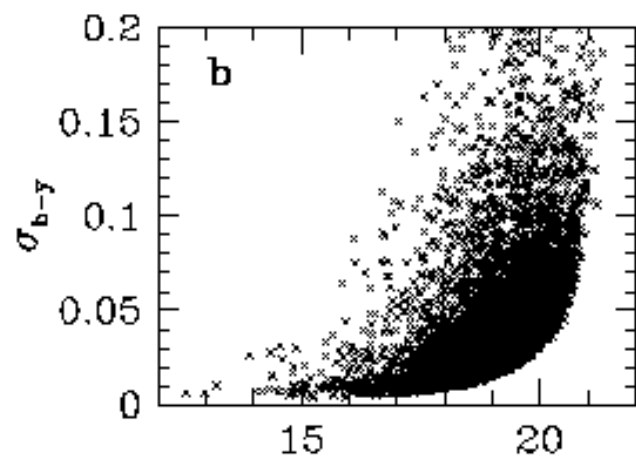
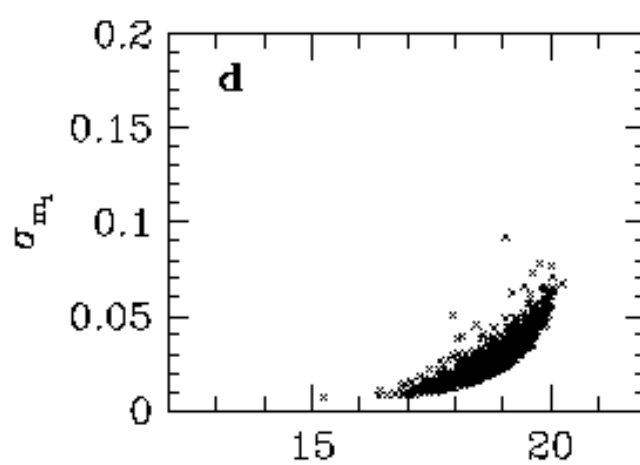
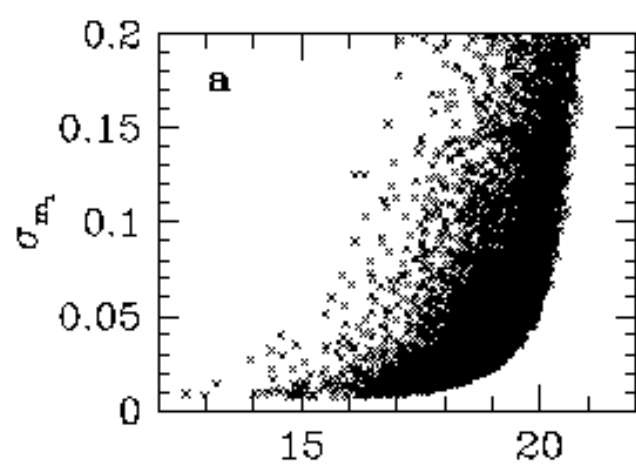


Table 2. Sample of Objects in  $\omega$  Cen

ID	$(b - y)$	$\sigma_{b-y}$	$V$	$\sigma_V$	$(v - b)$	$\sigma_{v-b}$	$m_1$	$M_V$
O 1	0.856	0.009	12.573	0.008	0.931	0.012	0.075	-1.659
O 2	0.834	0.009	13.104	0.008	0.081	0.010	-0.753	-1.128
O 3	0.769	0.012	13.640	0.008	0.205	0.014	-0.564	-0.592
O 4	0.602	0.010	13.834	0.008	0.608	0.013	0.006	-0.398
O 5	0.657	0.009	13.990	0.008	0.675	0.012	0.018	-0.242
O 6	0.693	0.010	14.049	0.009	0.836	0.013	0.143	-0.183
O 7	0.647	0.008	14.145	0.007	0.718	0.011	0.071	-0.087
O 8	0.638	0.011	14.177	0.009	0.189	0.013	-0.449	-0.055
O 9	0.724	0.012	14.236	0.008	0.811	0.012	0.087	0.004
O 10	0.652	0.009	14.333	0.008	0.687	0.011	0.035	0.101

Note. — **The complete table will be given in the electronic version of the *Astronomical Journal*.** Data with  $V > 16.4$  are from the longer exposures in Table 1, whereas data with  $V < 16.4$  comes from the 300s exposures.

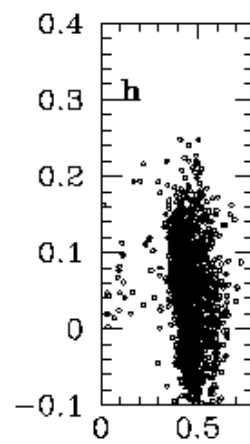
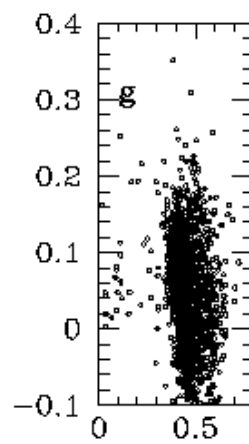
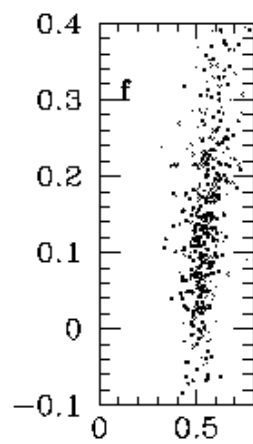
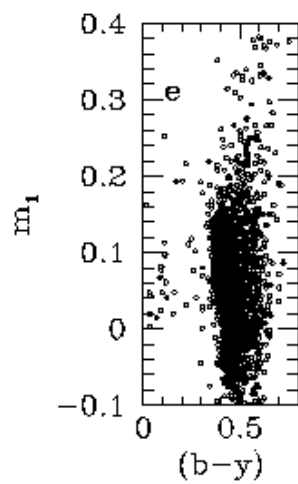
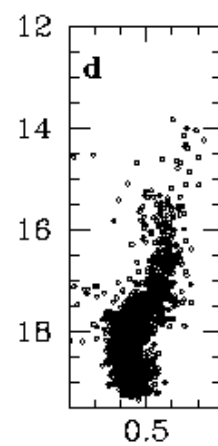
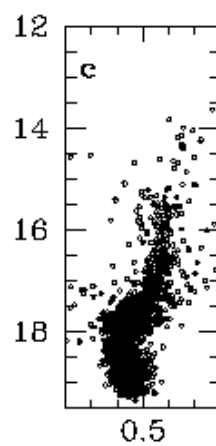
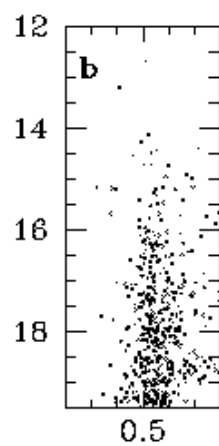
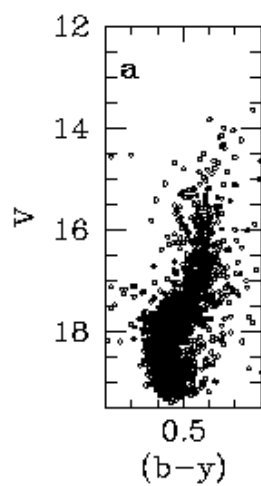


Table 3. Objects in the Off-Cluster Field

ID	$(b - y)$	$\sigma_{b-y}$	$V$	$\sigma_V$	$(v - b)$	$\sigma_{v-b}$	$m_1$
F 1	0.511	0.005	12.699	0.002	0.498	0.011	-0.013
F 2	0.409	0.020	13.211	0.021	0.678	0.008	0.269
F 3	0.522	0.003	14.121	0.002	2.529	0.035	2.007
F 4	0.853	0.004	14.152	0.003	1.349	0.007	0.496
F 5	0.838	0.004	14.212	0.002	1.390	0.009	0.552
F 6	0.495	0.022	14.276	0.009	0.711	0.021	0.216
F 7	0.716	0.006	14.409	0.004	0.989	0.007	0.273
F 8	0.554	0.006	14.429	0.004	0.720	0.007	0.166
F 9	0.533	0.004	14.494	0.002	0.780	0.012	0.247
F 10	0.463	0.006	14.540	0.004	3.466	0.045	3.003

Note. — **The complete table will be given in the electronic version of the *Astronomical Journal*.**

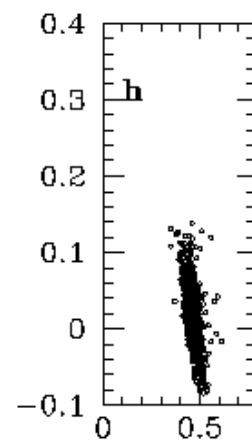
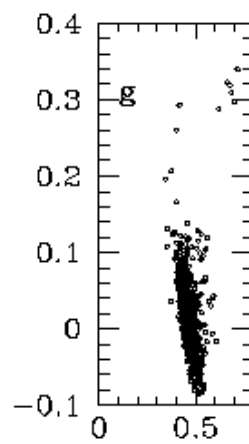
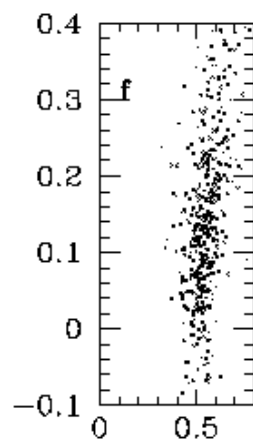
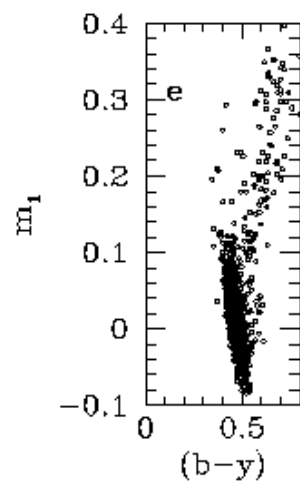
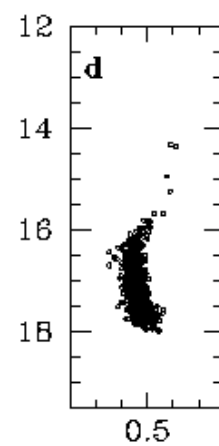
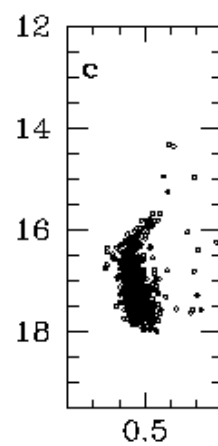
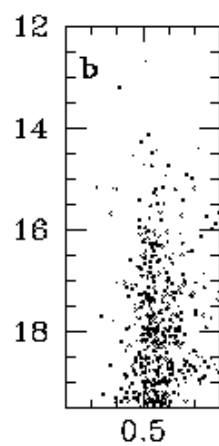
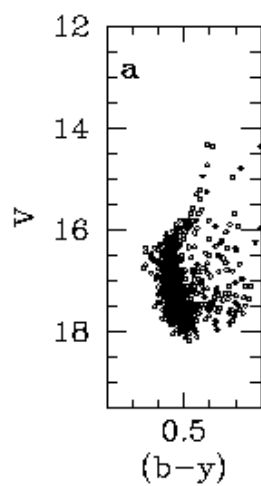


Table 4. Sample of Objects in NGC 6397

ID	$(b - y)$	$\sigma_{b-y}$	$V$	$\sigma_V$	$(v - b)$	$\sigma_{v-b}$	$m_1$	$M_V$
N 1	2.438	0.019	13.353	0.003	0.502	0.019	-1.936	0.650
N 2	0.593	0.009	14.324	0.005	0.635	0.008	0.042	1.620
N 3	0.610	0.007	14.358	0.004	0.594	0.007	-0.016	1.655
N 4	0.798	0.008	14.370	0.005	1.078	0.009	0.280	1.666
N 5	0.592	0.017	14.734	0.010	0.613	0.017	0.021	2.030
N 6	0.721	0.007	14.801	0.004	0.947	0.008	0.226	2.098
N 7	0.573	0.007	14.950	0.004	0.609	0.010	0.036	2.247
N 8	0.692	0.007	14.976	0.004	2.469	0.037	1.777	2.273
N 9	0.561	0.019	15.220	0.013	0.763	0.019	0.202	2.516
N 10	0.588	0.007	15.244	0.004	0.582	0.008	-0.006	2.540

Note. — **The complete table will be given in the electronic version of the *Astronomical Journal*.**

